Propagating Bloch bound states with orbital angular momentum above the light line in the array of dielectric spheres

Evgeny N. Bulgakov[1,2] **and Almas F. Sadreev**[1,*]

[1]*Kirensky Institute of Physics, Federal Research Center KSC SB RAS, 660036 Krasnoyarsk, Russia*
[2]*Siberian State Aerospace University, Krasnoyarsk, Russia*
Corresponding author: almas@tnp.krasn.ru

We present propagating Bloch bound states in the radiation continuum with orbital angular momentum in an infinite linear periodical array of dielectric spheres. The bound states in the continuum demonstrate a giant Poynting vector spiraling around the array. They can be excited by a plane wave with incident linear polarization with a small tilt relative to the axis of the array. © 2017 Optical Society of America

1. INTRODUCTION

Recently, periodical structures like arrays of rods have attracted attention with regard to the bound states in the radiation continuum (BSC) [1–18]. These BSC solutions are homogeneous along the axis of the rods and localized in the direction normal to the plane of the array. Their discrete eigenfrequencies are embedded into the radiation continuum, that is, they settle above the light line. Several mechanisms were elaborated for the BSCs, among them the symmetry protection, Fabry–Perot, and the mechanism of full destructive interference, which were outlined recently in the review by Hsu *et al.* [19]. The majority of the BSCs represents standing waves with a null Bloch vector. However, propagating Bloch BSCs were also reported [11,15,18].

BSCs were shown to exist in the one-dimensional infinite array of dielectric spheres [20–23]. The array is remarkable because of its rotational symmetry, which gives rise to preservation of the orbital angular momentum (OAM). The diffraction continua given by vector cylindric modes [20] are also specified by the corresponding OAM given by the integer m. As a result, the BSCs can be considered independently in each sector m.

The angular momentum is composed of the spin angular momentum (SAM) and OAM describing the polarization and the phase structure distribution of EM fields, respectively. The OAM of EM fields has been the focus of research since Padgett, Courtial, and Allen investigated the mechanism of the OAM in laser modes [24,25]. In Ref. [21], we have shown that quasi-BSCs with OAM can be excited by light beam with circular polarization. If the frequency of incident light is close

to the BSC frequency, the electromagnetic field in the near zone of the array blows up [21,26–28]. Consequently, a giant Poynting vector current circulating around the array was demonstrated [21]. In the present paper, we consider the Bloch BSCs with OAM, which propagate along the array of dielectric spheres. They also demonstrate a giant Poynting vector now spiraling around the array. In contrast to the standing quasi-BSCs with OAM, which can only be excited by a plane wave with circular polarization, the propagating quasi-BSC with OAM can be excited by plane wave with incident *linear polarization* with tilt relative to the array axis.

2. BLOCH PROPAGATING BSCS

Our numerical approach is based on the analytical theory by Linton *et al.*, who managed to obtain a multipole relation in a closed form that is suitable for finding guided modes in the array of dielectric spheres below the light line [29]. Their approach was also successfully applied for solutions embedded into the lowest diffraction continua, bound states in the continuum [20]. In particular, we revealed Bloch waves with a non-zero Bloch vector β, which can be interpreted as waves guided along the array similar to the Bloch solutions in a periodic array of infinitely long dielectric rods [11,15,18]. BSCs with OAM $|m| \neq 0$ but $\beta = 0$ were reported earlier [21]. Here we present Bloch BSCs that have both $\beta \neq 0$ and $m = \pm 1$ embedded into the first diffraction continuum $n = 0$ but below the next continua with $n > 0$ where the cylindrical continua are classified by the integer $n = 0, 1, 2, \ldots$ and are given by the scalar function [30]

$$\psi_{mn} = H_m^{(1)}\left(\sqrt{k_0^2 - (\beta + 2\pi n)^2}\, r\right) e^{im\phi + i(\beta + 2\pi n)z}, \qquad \textbf{(1)}$$

where $H_m^{(1)}$ is the Hankel function of the first order. In what follows, the radius and the wave length $2\pi/\beta$ are measured in terms of the period of the array h, and the frequency k_0 is measured in terms of c/h, where c is the light velocity.

The Maxwell equations can be written as an analogue of the Lippmann–Schwinger equation:

$$\widehat{L}\vec{\psi} = \vec{\psi}_{\mathrm{inc}}, \qquad \textbf{(2)}$$

where the structure of the matrix $\widehat{L}$ is given in Refs. [20,29] and the columns $\vec{\psi}$ are composed of the amplitudes of the expansion over vector spherical harmonics. The incident plane wave can be written in the following form:

$$\vec{\psi}_{inc} = \vec{\psi}^{\mathrm{TE}} + \kappa \vec{\psi}^{\mathrm{TM}}. \qquad \textbf{(3)}$$

The TE and TM modes of electromagnetic field are expressed through function ψ [21,30], in particular, for the TE mode $H_z = \psi$ and for the TM mode $E_z = \psi$. The factor κ controls the polarization of the incident wave. In particular, the imaginary $\kappa = i$ gives a circular polarization, while the real κ defines a linear polarization of the incident field.

For fixed permittivity of the spheres $\varepsilon = 10$, the BSC solution is sought in the space of three parameters: the radius of the spheres R, the frequency k_0, and the Bloch vector β by finding the real poles of the matrix $\widehat{L}$, as shown in Fig. 1. That numerical procedure is described in detail in Refs. [20–22]. For the degenerate Bloch BSC with $m = \pm 1$, we obtain $\beta_c = 1.302$, as shown in Fig. 1, provided that the other parameters are tuned to the BSC point given in the figure caption. Then, the BSC solution is given by the homogeneous part of Eq. (2), $\widehat{L}\vec{\psi}_c = 0$.

The z-component of the magnetic field of the BSC solution is shown in Fig. 2. All other solutions with different Bloch vectors $\beta \neq \beta_c$ leak into the radiation continuum $n = 0$ as seen from Fig. 1, but they still can serve in a guiding capacity with high quality factor [22]. Figure 3 shows that the frequency and
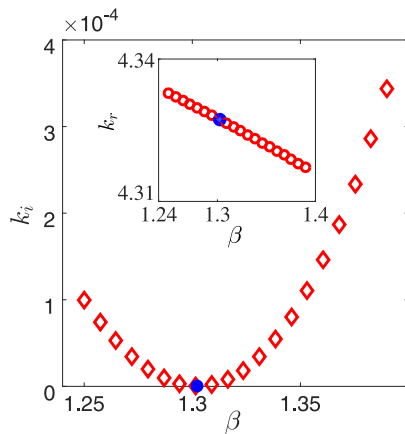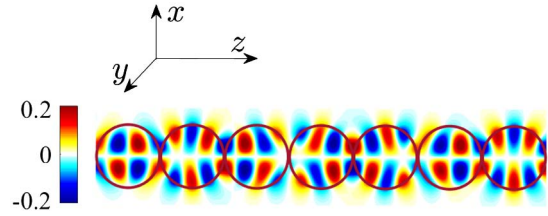

Fig. 2. Propagating Bloch BSC with the Bloch vector $\beta_c = 1.302$, frequency $k_{0c} = 4.327$, and OAM $m = 1$ calculated for spheres with $\varepsilon = 10, R_c = 0.489$. The real part of the electromagnetic field component H_z is shown.
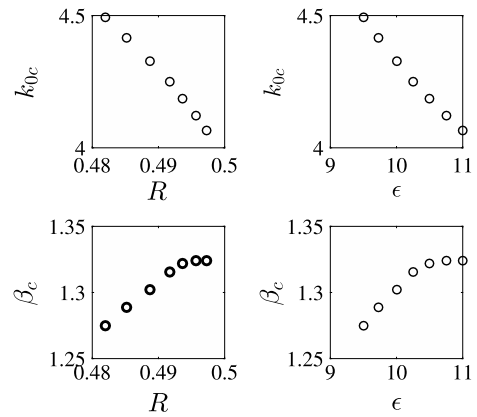

Fig. 3. BSC frequency k_{0c} and Bloch BSC vector β_c versus radius and permittivity of dielectric spheres.

the Bloch vector of the BSC can be tuned by the radius and permittivity of the dielectric spheres.

Previously, we have demonstrated the transfer of SAM of a plane wave with circular polarization into OAM of a standing BSC [21]. Here we demonstrate that a wave with linear polarization can excite the propagating Bloch quasi-BSC with $m = \pm 1$. Specifically, the incident wave was applied as follows. The wave vector of the incident plane wave was chosen to be $\vec{k} = (k_x, 0, \beta)$, where $k_x = \sqrt{k_{0c}^2 - \beta^2}, \beta = \beta_c + 0.005$. The polarization is given by parameter κ in Eq. (3). In particular for $\kappa = 0$, the incident wave is a TE mode in the plane (x, z). However, as soon as κ is real, the polarization of electric field tilts relative to the plane (x, z).

In the vicinity of the BSC point, the solution is mainly given by the eigenfunction of the matrix $\widehat{L}$ whose complex eigenvalue L_c is closest to zero (the condition $L_c = 0$ defines the BSC solution) [21]:

$$\vec{\psi} \approx B_{m=1}\vec{X}_{\mathrm{BSC}}^{m=1} + \vec{X}_{\mathrm{BSC}}^{m=-1}, \qquad \textbf{(4)}$$

where

$$B_{m=\pm 1} = \frac{1}{L_c}(D^{\mathrm{TE}} \pm \kappa D^{\mathrm{TM}}), \qquad D^\sigma = \vec{Y}_{\mathrm{BSC}}^+ \vec{\psi}^\sigma, \qquad \textbf{(5)}$$

where $\sigma = $ TE, TM labels the polarization of electromagnetic field. $\vec{Y}_{\mathrm{BSC}}^+$ and $\vec{X}_{\mathrm{BSC}}$ are the left and right eigenvectors of the matrix:

Fig. 1. Imaginary (main plot) and real (inset) parts of the complex eigenfrequency of propagating solution with $m = \pm 1$ versus the Bloch vector β for other relevant parameters tuned to the BSC point $k_{0c} = 4.327, R = 0.489, \varepsilon = 10$. The closed circle marks the BSC Bloch vector β_c.
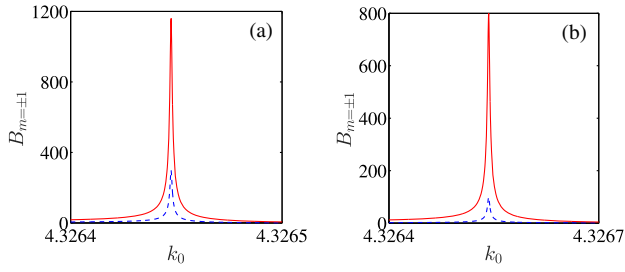
Fig. 4. Enhancement factor $B_{m=1}$ (dashed line) and $B_{m=-1}$ (solid line) versus frequency for the parameters listed in Fig. 1, $\beta = \beta_c + 0.0062$, and (a) $\kappa = 1$ and (b) $\kappa = 0.5$. In the case of $\kappa = -1, -0.5$, the dashed and solid lines are interchanged.

$$\widehat{L}\vec{X}_{\mathrm{BSC}} = L_c\vec{X}_{\mathrm{BSC}}, \quad \vec{Y}^+_{\mathrm{BSC}}\widehat{L} = L_c\vec{Y}^+_{\mathrm{BSC}}. \tag{6}$$

Both eigenvectors are decomposed at subspaces $m = \pm 1$. Therefore, the amplitude $B_{m=\pm 1}$ can be interpreted as responses with OAM $m = \pm 1$ to the incident wave with linear polarization in the vicinity of the BSC point as dependent on the sign of κ. In particular, the case $\kappa > 0$ is shown in Fig. 4(a), which demonstrates a resonant enhancement in the vicinity of the BSC frequency $k_{0c} = 4.327$. More importantly, Fig. 4 shows that the amplitudes $B_{m=\pm 1}$ are substantially different
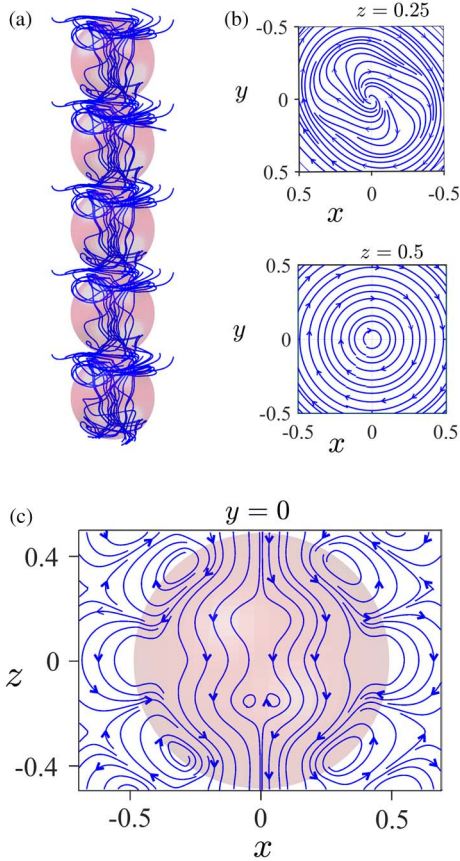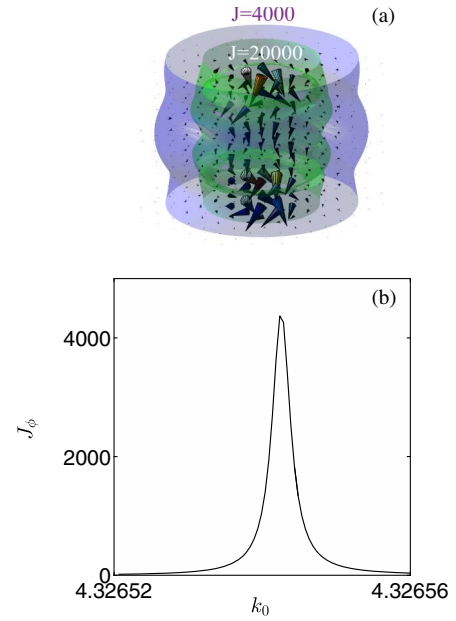

Fig. 6. (a) Iso-surfaces of Poynting vector at two selected values and (b) value of azimuthal component of the Poynting vector normalized to the incident wave around the spheres at distance $r = 0.588$ from the center of sphere and $z = 0$.

for a plane wave with oblique incidence. The change of the sign of κ interchanges priority of $B_{m=\pm 1}$, which in turn changes the direction of spiraling.

The spiraling currents nearby the array become giant, because of enhancement of the EM fields for the frequency close to the BSC frequency, as shown in Fig. 5. This figure is complemented by Figs. 6(a) and 6(b), with iso-surfaces of absolute value and the azimuthal component in Fig. 6(b) of the Poynting vector, which demonstrates the enhancement.

The next unique property of the BSC is related to the Fano resonance collapse [26,31] that reflects in the resonant features of the cross sections of the array in the vicinity of the BSC frequency. Similar to the BSCs with $\beta = 0$ and $m \neq 0$, which were presented in Ref. [21], the Bloch BSC with OAM demonstrates resonant features shown in Fig. 7.
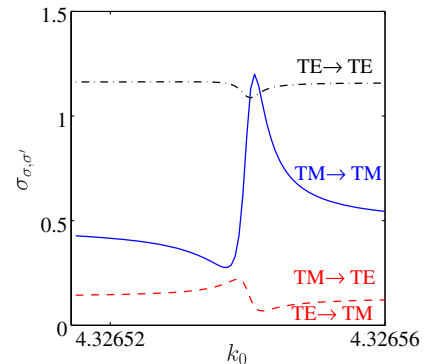

Fig. 5. (a) Streamlines of Poynting vector, (b) currents in the x, y plane at selected slices along the array axis $z = 0.25$ (inside the sphere) and $z = 0.5$ (between spheres), and (c) currents in the x, z plane at selected slices $y = 0$.

Fig. 7. Total cross-section for scattering of plane wave by the array in the vicinity of the Bloch BSC with OAM at $\beta = \beta_c + 0.0062$.

3. DISCUSSIONS AND SUMMARY

The standing BSCs with OAM $m = \pm 1$ but $\beta = 0$ and $m = \pm 2$ and the propagating Bloch BSCs with $\beta \neq 0$ but with zero OAM were previously predicted due to the axial symmetry of the array [20,22]. In the present paper, we have filled the gap between the two by finding propagating Bloch BSCs with both $\beta \neq 0$ and OAM $m = \pm 1$ for dielectric particles with the permittivity around ten. The Bloch vector β_c can be tuned by variation of the permittivity, as shown in Fig. 3. Although we revealed only $m = \pm 1$ BSCs, in general, there is no restriction for the Bloch BSCs with OAM $|m| > 1$. To the best of our knowledge, the BSCs with OAM guided along the array have not been previously proposed as a possible fundamental effect for device applications. One of the most important possible applications is lasing through the BSC, as was demonstrated in Refs. [32–34]. The principal feature of lasing by the array of dielectric spheres is that the laser beam carries the OAM without the use of special chiral symmetry broken media [35–37]. The next important result is excitation of propagating quasi-BSCs with OAM by linearly polarized plane waves.

In practice, the array holds a finite number of spheres. Preliminary simulations show that in a finite array of spheres, the BSCs become quasi-BSCs [21]. Nevertheless the giant enhancement of scattered field in the near zone holds in a finite array too though the enhancement factor decays towards the ends of the array.

REFERENCES

1. A.-S. Bonnet-Bendhia and F. Starling, "Guided waves by electromagnetic gratings and non-uniqueness examples for the diffraction problem," Math. Methods Appl. Sci. **17**, 305–338 (1994).
2. D. V. Evans and R. Porter, "Trapping and near-trapping by arrays of cylinders in waves," J. Eng. Math. **35**, 149–179 (1999).
3. O. Cohen, B. Freedman, J. W. Fleischer, M. Segev, and D. N. Christodoulides, "Grating-mediated waveguiding," Phys. Rev. Lett. **93**, 103902 (2004).
4. S. P. Shipman and S. Venakides, "Resonant transmission near nonrobust periodic slab modes," Phys. Rev. E **71**, 026611 (2005).
5. D. C. Marinica, A. G. Borisov, and S. V. Shabanov, "Bound states in the continuum in photonics," Phys. Rev. Lett. **100**, 183902 (2008).
6. W. J. Hsueh, C. H. Chen, and C. H. Chang, "Bound states in the continuum in quasiperiodic systems," Phys. Lett. A **374**, 4804–4807 (2010).
7. C. W. Hsu, B. Zhen, J. Lee, S.-L. Chua, S. G. Johnson, J. D. Joannopoulos, and M. Soljačić, "Observation of trapped light within the radiation continuum," Nature **499**, 188–191 (2013).
8. C. W. Hsu, B. Zhen, S.-L. Chua, S. G. Johnson, J. D. Joannopoulos, and M. Soljačić, "Bloch surface eigenstates within the radiation continuum," Light Sci. Appl. **2**, 1 (2013).
9. S. Weimann, Y. Xu, R. Keil, A. E. Miroshnichenko, A. Tünnermann, S. Nolte, A. A. Sukhorukov, A. Szameit, and Y. S. Kivshar, "Compact surface Fano states embedded in the continuum of the waveguide arrays," Phys. Rev. Lett. **111**, 240403 (2013).
10. Y. Yang, C. Peng, Y. Liang, Z. Li, and S. Noda, "Analytical perspective for bound states in the continuum in photonic crystal slabs," Phys. Rev. Lett. **113**, 037401 (2014).
11. E. N. Bulgakov and A. F. Sadreev, "Bloch bound states in the radiation continuum in a periodic array of dielectric rods," Phys. Rev. A **90**, 053801 (2014).
12. Z. Hu and Y. Y. Lu, "Standing waves on two-dimensional periodic dielectric waveguides," J. Opt. **17**, 065601 (2015).
13. M. Song, H. Yu, C. Wang, N. Yao, M. Pu, J. Luo, Z. Zhang, and X. Luo, "Sharp Fano resonance induced by a single layer of nanorods with perturbed periodicity," Opt. Express **23**, 2895–2903 (2015).
14. C.-L. Zou, J.-M. Cui, F.-W. Sun, X. Xiong, X.-B. Zou, Z.-F. Han, and G.-C. Guo, "Guiding light through optical bound states in the continuum for ultra high-Q microresonators," Laser Photon. Rev. **9**, 114–119 (2015).
15. Y.-J. Hung and I.-S. Lin, "Visualization of Bloch surface waves and directional propagation effects on one-dimensional photonic crystal substrate," Opt. Express **24**, 16003–16009 (2016).
16. Y. Wang, J. Song, L. Dong, and M. Lu, "Optical bound states in slotted high-contrast gratings," Opt. Lett. **33**, 2472–2479 (2016).
17. C. Blanchard, J.-P. Hugonin, and C. Sauvan, "Fano resonances in photonic crystal slabs near optical bound states in the continuum," Phys. Rev. B **94**, 155303 (2016).
18. L. J. Yuan and Y. Y. Lu, "Propagating Bloch modes above the light line on a periodic array of cylinders," J. Phys. B **50**, 05LT01 (2017).
19. C. W. Hsu, B. Zhen, A. D. Stone, J. D. Joannopoulos, and M. Soljačić, "Bound states in the continuum," Nat. Rev. Mater. **1**, 16048 (2016).
20. E. N. Bulgakov and A. F. Sadreev, "Light trapping above the light cone in one-dimensional array of dielectric spheres," Phys. Rev. A **92**, 023816 (2015).
21. E. N. Bulgakov and A. F. Sadreev, "Transfer of spin angular momentum of an incident wave into orbital angular momentum of the bound states in the continuum in an array of dielectric spheres," Phys. Rev. A **94**, 033820 (2016).
22. E. N. Bulgakov and D. N. Maksimov, "Light guiding above the light line in arrays of dielectric nanospheres," Opt. Lett. **41**, 3888–3891 (2016).
23. E. N. Bulgakov and A. F. Sadreev, "Trapping of light with angular orbital momentum above the light cone in a periodic array of dielectric spheres," Adv. Electromagn. **6**, 1 (2017).
24. M. Padgett, J. Courtial, and L. Allen, "Light's orbital angular momentum," Phys. Today **57**(5), 35–40 (2004).
25. A. M. Yao and M. J. Padgett, "Orbital angular momentum: origins, behavior and applications," Adv. Opt. Photon. **3**, 161–204 (2011).
26. A. F. Sadreev, E. N. Bulgakov, and I. Rotter, "Bound states in the continuum in open quantum billiards with a variable shape," Phys. Rev. B **73**, 235342 (2006).
27. M. Zhang and X. Zhang, "Ultrasensitive optical absorption in graphene based on bound states in the continuum," Sci. Rep. **5**, 8266 (2015).
28. J. W. Yoon, S. H. Song, and R. Magnusson, "Critical field enhancement of asymptotic optical bound states in the continuum," Sci. Rep. **5**, 18301 (2015).
29. C. M. Linton, V. Zalipaev, and I. Thompson, "Electromagnetic guided waves on linear arrays of spheres," Wave Motion **50**, 29–40 (2013).
30. J. A. Stratton, *Electromagnetic Theory* (McGraw-Hill, 1941).
31. C. S. Kim, A. M. Satanin, Y. S. Joe, and R. M. Cosby, "Resonant tunneling in a quantum waveguide: effect of a finite-size attractive impurity," Phys. Rev. B **60**, 10962–10970 (1999).
32. Z. Zhang, Y. Li, W. Liu, and J. Yang, "Controllable lasing behavior enabled by compound dielectric waveguide grating structures," Opt. Express **24**, 19458–19466 (2016).
33. A. Kodigala, T. Lepetit, Q. Gu, B. Bahari, Y. Fainman, and B. Kanté, "Bound state in the continuum nanophotonic laser," in *CLEO: Science and Innovations* (2016), paper SM4E.
34. P. Miao, Z. Zhang, J. Sun, W. Walasik, S. Longhi, N. M. Litchinitser, and L. Feng, "Orbital angular momentum microlaser," Science **353**, 464–467 (2016).
35. Y. Gorodetski, A. Drezet, C. Genet, and T. W. Ebbesen, "Generating far-field orbital angular momenta from near-field optical chirality," Phys. Rev. Lett. **110**, 203906 (2013).
36. R. Dall, M. D. Fraser, A. S. Desyatnikov, G. Li, S. Brodbeck, M. Kamp, C. Schneider, S. Höfling, and E. A. Ostrovskaya, "Creation of orbital angular momentum states with chiral polaritonic lenses," Phys. Rev. Lett. **113**, 200404 (2014).
37. N. Yu and F. Capasso, "Optics with designer metasurfaces," Nat. Mater. **13**, 139–150, 2014.